Int J Adv Manuf Technol (2017) 91:1117–1128
DOI 10.1007/s00170-016-9791-x

ORIGINAL ARTICLE

Prediction for multi-index constrained forming limit in shear bending process of Ti-alloy thin-walled tube under differential temperature fields

Jing Yan [1,2,3] · **Wei Wu** [1,2,3] · **Bingtong Xu** [1,2,3]

Received: 4 July 2016 / Accepted: 18 November 2016 / Published online: 1 December 2016

Abstract Predictions for multi-index constrained forming limits and forming limits of Ti-alloy thin-walled tubes have become key problems urgently in need of solutions in order to improve forming potential in their shear bending processes under differential temperature fields. To address this, a method for predicting this type of forming limits was presented by coupling a thermal-mechanical-coupled finite element model for simulating these bending processes, with an energy model for the tubes' shear-enforced plastic wrinkling predictions and utilizing the response surface designs. Reliable multi-index response surface models corresponding to the wrinkling, the thinning, and the flattening were developed for these TA2 Ti-alloy tubes' shear bending processes, and their multi-index constrained forming limits were predicted. This found that forming limits, i.e., the maximum moving die displacements depend on the over-thinning or over-flattening for the present conditions. The smaller the values of the outer corner radius, the smaller both the feasible region ranges of the bending die cavity radius and/or the mandrel diameter and these forming limits. When the value of the outer corner radius is a half of the mandrel diameter and the values of the inner corner radius are from 4 to 6 mm; their feasible region ranges are the maximum. The effects of the feasible region of the bending die cavity radius on these forming limits are larger than the mandrel diameter. The moving die displacements located in the vertexes of their feasible regions are the maximum.

Keywords Forming limits · Multi-index constraint · Ti-alloy thin-walled tube · Shear bending · Differential temperature fields

1 Introduction

As a compact, light-weight component with high strength and performance, Ti-alloy thin-walled tubes with ultra-small bend radii (bend radii and tube diameter ratios < 1) integrate structural and material advantages in a way that makes them be widely applicable to aerospace, aviation, and related high technology industries. Tube bending is a key technology for manufacturing tube parts, and it has shown a tendency to focus its development on these Ti-alloy thin-walled tubes [1]. In contrast to the existing rotary draw bending [2–5] and push bending [6], a shear bending process under differential temperature fields, as shown in Fig. 1, has provided an innovative solution to enable the manufacturing of these Ti-alloy thin-walled tubes while decreasing yield strength and improving formability.

In Fig. 1, a tube is bent by a shear force. After passing along die corners, its bend deformation zone transforms into a vertical segment that enables the transfer of shear force to the tube blank. Its extrados is subjected to a tension stress and its vertical segment is subjected to a shear stress. These stress conditions can possibly produce defects including shear-enforced wrinkling, over-thinning of wall thickness, and over-flattening of cross section. A tube shear structure enables inner corner radius to match randomly outer corner radius, and the larger the values of moving die displacement, the larger the values of vertical segment length. Probabilities of these defects grow

✉ Jing Yan
yanjing2008win@163.com

[1] Aeronautical Key Laboratory for Plastic Forming Technology, Beijing 100024, China

[2] Beijing Key Laboratory of Digital Plastic Forming Technology and Equipment, Beijing 100024, China

[3] Beijing Aeronautical Manufacturing Technology Research Institute, Beijing 100024, China

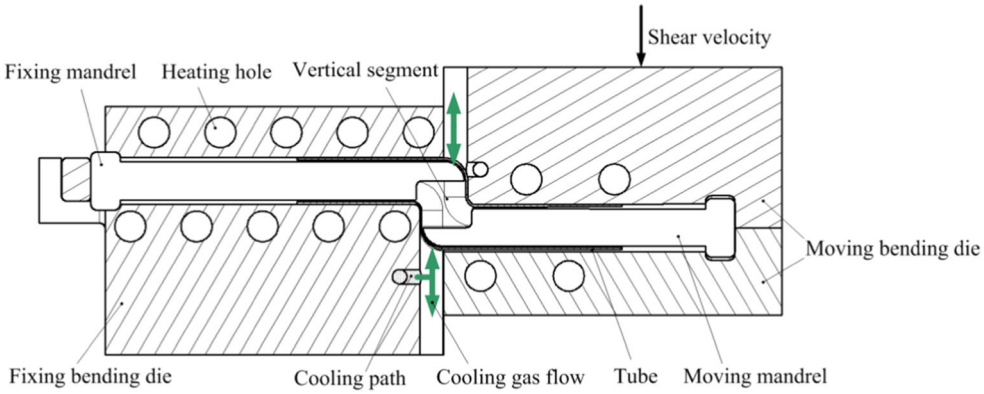

Fig. 1 Shear bending process of Ti-alloy thin-walled tube under differential temperature fields

with the increases of displacement and the decreases of corner radius. Tube's forming limits are determined by three forming indices including the shear-enforced wrinkling, the thinning, and the flattening. Thus, the predictions of multi-index constrained forming limits and the forming limits of Ti-alloy thin-walled tubes have become key problems urgently need to be solved for improving their forming potentials in their shear bending processes under differential temperature fields. However, up to now, a great deal of research about the forming limit predictions has been carried out mainly in the problems under the single index constraint [7–23]; there are hardly any published studies on the predictions of these multi-index constrained ones in these shear bending processes.

Over the last several decades, three kinds of methodologies have been respectively used for predicting forming limits in sheet/tube metal forming processes. These consist of an analytical approach, an experimental approach, and a numerical simulation. Forming limits have been defined as limit forming parameters corresponding to the critical forming indices.

1. The analytical approach is based on the mechanics of metal plastic deformation or the plastic instable theory. The instable criterions have been analyzed for predicting the forming limits in these metal forming processes [7–14]. The classical or modified M-K models have been used for predicting the limit fracture stresses or strains [7–11], e.g., Li et al. [8] developed the forming limit diagrams (FLDs) in the hot stamping processes of 22MnB5 steel plates, and Hashemi et al. [9] developed the FLDs in the aluminum tube hydroforming processes. Sun et al. [12] analyzed the critical wrinkling axial loads in the tube axial compressive processes by using the energy method. Yang et al. [13] analyzed the tube wrinkling minimum bending radii by using the wrinkling energy model. Liu et al. [14] analyzed the critical internal pressures of the side walls wrinkling in the hydroforming processes of the thin-walled tube tee-joints.
2. The experimental approach is based on the specific or standard experiments. The critical fracture/wrinkling strains in these experimental processes have been measured online, and the fracture/wrinkling FLDs have been developed [15–18]. Tao et al. [17] determined the FLDs of Al/Cu clad plates by using the digital optical deformation measurement system.
3. The numerical simulation is based on the finite element (FE) models for simulating these forming processes. The relationships between the forming parameters and the forming indices have been established enabling the forming limit predictions [19–24]. Li et al. [19] combined the Cockroft-Latham fracture model with the FE model for simulating the hot stamping processes of 22MnB5 steel plates and predicted the plate limit fracture strain. Xiao et al. [21] developed the FE model for simulating the rotary draw bending processes of H96 brass double-ridged rectangular tubes; the minimum bending radius based on the cross-sectional distortion has been predicted by using the orthogonal regression method. Nguyen et al. [22] combined the modified maximum force fracture model and the FE model for simulating the incremental forming processes and predicted the material maximum heights by using the single factor rotation method. Yan et al. [24] combined the FE model for simulating the rotary draw bending processes of Al-alloy thin-walled tubes with the wrinkling energy model and presented the search method for multi-index constraint forming limits. Their minimum bending radii under the multi-index constraints have been determined. Otherwise, the methods for building these relationships between the forming parameters and the indices also include the artificial neural network [25], the genetic algorithm [26], and the response surface design [27]. The response surface models have been presented by the polynomial regression equations unlike the other both methods describing these relationships as the "black boxes", and they are apt to optimize forming parameters enabling determinations of the forming limits accurately and effectively.

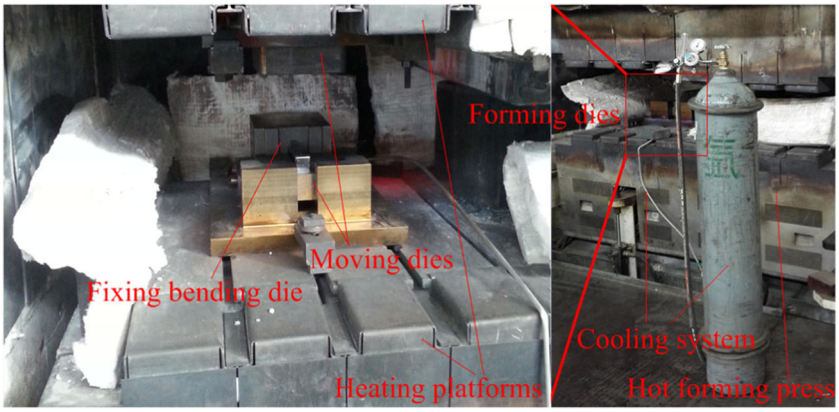

Fig. 2 Shear bending apparatus of Ti-alloy thin-walled tube under differential temperature fields

Ti-alloy thin-walled tubes are covered by the combination dies in their shear bending processes under differential temperature fields, and thus, it is difficult to measure their forming limits online and describe the relationships between the forming parameters and the forming indices completely by using the response surface models established only based on the experimental results. Forming limits obtained only by using analytical approach cannot consider the effects of several vital parameters on tube shear plastic deformation behaviors, such as the complicated thermal-mechanical-coupled dynamic contact behaviors between the tubes and the different dies. It is also difficult to solve these complicated contact problems by using an implicit FE method due to the deteriorated convergence in each iteration procedure. Combination of the explicit thermal-mechanical-coupled FE models for simulating these shear bending processes with the energy model has been able to predict the shear-enforced wrinkling reliably in ref. [28]. Thus, a method for predicting the multi-index constrained forming limits was presented by coupling the thermal-mechanical-coupled finite element model for simulating these bending processes, with the energy model for the tubes' shear enforced plastic wrinkling predictions and utilizing the response surface designs. The reliable multi-index response surface models corresponding to the wrinkling, the thinning, and the flattening were developed for these TA2 Ti-alloy thin-walled tubes' shear bending processes, and their forming limits were predicted.

2 Research methodology

2.1 Forming indices

The forming defects of Ti-alloy thin-walled tubes in their shear bending processes under differential temperature fields include the over-thinning, the over-flattening, and the shear enforced plastic wrinkling.

The maximum thinning ratio I_t is used to define the thinning degrees as follows:

$$I_t = (t - t')/t \tag{1}$$

where t is the initial tube wall thickness, and t' is the minimum wall thickness after bending. The over-thinning is judged by the critical value of $I_t \geq 0.25$.

The maximum ovality I_d is used to define the flattening degrees as follows:

$$I_d = (D - D')/D \tag{2}$$

Table 1 TA2 tube thermal physical properties [29]

No.	Preheating temperature, T (°C)	Heat capacity, ω (J kg^{-1} °C^{-1})	Conduction coefficient, λ(W m^{-1} °C^{-1})	Thermal expansion coefficient,η (10–6 °C^{-1})	Elastic module, E (GPa)
1	25	–	19.3	–	52
2	100	503	18.9	8.9	–
3	200	545	18.4	9.3	–
4	300	566	18	9.8	86
5	400	587	18	10.2	82
6	500	628	18	10.4	80
7	600	670	18	10.5	–

Table 2 TA2 tube shear stress constitutive parameters [30]

No.	Preheating temperature, T (°C)	Strength coefficient, K(T) (MPa)	Strain hardening index, n(T)	Strain rate sensitive coefficient, m(T)
1	25	450.54	0.242	–
2	300	173.94	0.220	0.017
3	350	127.78	0.136	0.037
4	400	115.97	0.120	0.028
5	450	98.43	0.099	0.013
6	500	90.00	0.088	0.020

where D is the initial tube diameter and D' is the minimum diameter after bending. The over-flattening is judged by the critical value of $I_d \geq 0.05$.

The wrinkling factor I_w for describing the shear enforced wrinkling probabilities are defined as follows:

$$I_w = \Delta W / \Delta U_{min} \tag{3}$$

where ΔU_{min} is the minimum wrinkling energy of the wrinkling sensitive zone and $\Delta W$is the work done by the external force. The shear enforced wrinkling is judged by the critical value of $I_w \geq 1$, otherwise the stable forming occurs. The computational method of the wrinkling factor has been discussed in detail in ref. [28].

2.2 Experimental process

Shear bending experiments of the TA2 Ti-alloy thin-walled tubes under the differential temperature fields were performed, and the experimental apparatus included the forming dies, a cooling system, and a hot forming press, as shown in Fig. 2. A cooling gas source linked with the forming dies by a thin metal tube supplying the argon. The thermal physical properties of TA2 tube were listed in Table 1 [29]. The tube constitutive equations are $\overline{\sigma} = K(T)\overline{\varepsilon}^{n(T)}\dot{\overline{\varepsilon}}^{m(T)}$, where $\overline{\sigma}$ is the equivalent stress, $\overline{\varepsilon}$ is the equivalent strain, and $\dot{\overline{\varepsilon}}$ is the equivalent strain rate. The tube shear stress constitutive parameters (K(T), n(T), and m(T)) acquired by using the method described in ref. [30] and explained in Table 2 in detail.

A tube and the forming dies were heated by the press platforms, and their temperatures were measured by a thermocouple inserted in a fixing bending die. Transfer mechanisms were the heat conduction between the tube and the bending dies/mandrels (fixing and moving mandrel), the heat convection between the tube and its ambience, mainly the air and the cooling gas flow, and the thermal radiation between them. The corresponding heat transfer parameters were determined by referring to ref. [31], and the conduction coefficients λ_{td} between the tube and the dies were defined as follows:

$$\lambda_{td} = \frac{1}{\frac{1}{\lambda_1} + \frac{\delta'}{\lambda} + \frac{1}{\lambda_2}} \tag{4}$$

where δ' was the clearance between the tube and the bending dies/mandrels; λ_1 and λ_2 were the conduction coefficients between the clearance and either the tube surface or the die respectively; λ was the clearance conduction coefficient. In experimental processes, only the air was considered to exit in the clearances between the tube and the bending dies/mandrels because their oxide films were much thinner than the clearances.

The tube blank shown in Fig. 3 was used for prevention of wall thinning. The surfaces of both the half tube with the slope end and the die cavities were lubricated by an air dry solid film lubricant (T50) to decrease the friction coefficient between them, while the surfaces of the other half tube were unlubricated. The friction coefficients between the tube and the dies were determined

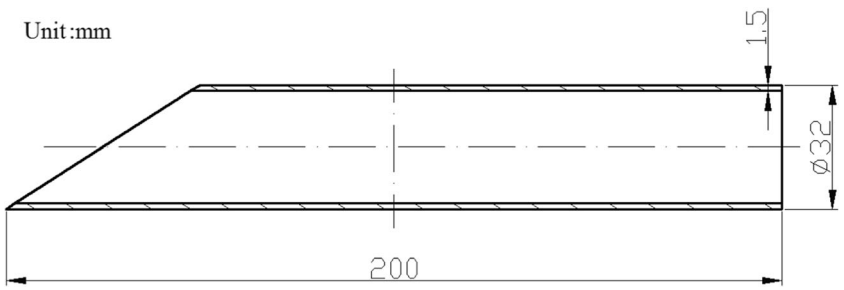

Fig. 3 Geometrical shape of tube blank

Table 3 Experimental parameters

Parameter	Value
Tube diameter, D (mm)	32.00
Tube wall thickness, t (mm)	1.50
Inner corner radius, r_i (mm)	4.00
Bending die cavity radius, R_b (mm)	16.65
Mandrel diameter, D_m (mm)	28.35
Outer corner radius, r_o (mm)	10.18–14.18
Bending speed, V (mm/s)	2.00
Preheating temperature, T (°C)	400.00
Ambient temperature, T' (°C)	25.00
Conduction coefficient between tube and forming dies, λ_{td} (W m^{-2} °C^{-1})	22,000
Unforced convection coefficient between tube and ambient, h_{ta} (W m^{-2} °C^{-1})	2
Compulsory convection coefficient between tube and ambient, h_{ta}' (W m^{-2} °C^{-1})	25–100
Tube radiation coefficient, p_t (W m^{-2} °C^{-1})	0.60
Die radiation coeffcient, p_d (W m^{-2} °C^{-1})	0.80
Friction coefficient between tube and fixing dies, μ_{tf}	0.05
Friction coefficient between tube and moving dies, μ_{tm}	0.20

by referring to ref. [32]. The experimental parameters were listed in Table 3.

Two kinds of mandrel structures were designed for manufacturing tube parts with the different values of the outer corner radius r_o. When $r_o = D_m/2$, the structure was shown in Fig. 4a, where D_m is the mandrel diameter; when $r_o < D_m/2$, in Fig. 4b, and $r_o = D_m/2\text{-}\delta$, where δ is the change of r_o. The experiments were performed based on a response surface design shown in Table 4 and the parameters listed in Table 3.

The experimental parts were shown in Fig. 5. All the tubes were no wrinkling. Their values of I_d were measured by using a vernier calipers. Then, they were divided in half along their symmetrical central planes and their values of I_t were measured by a centesimal meter. The measurement results were shown in Table 4.

Table 4 Response surface design of experiment

No.	Parameter		I_t	I_d
	Moving die displacement H (mm)	Outer corner radius r_o (mm)		
1.	30	12.15	0.261	0.044
2.	30	14.15	0.210	0.048
3.	35	10.15	0.376	0.067
4.	40	12.15	0.330	0.067
5.	35	12.15	0.295	0.060
6.	40	14.15	0.280	0.060
7.	40	10.15	0.405	0.098
8.	30	10.15	0.328	0.063
9.	35	14.15	0.254	0.054

2.3 Prediction method of multi-index constrained forming limits

2.3.1 Definitions of forming limits

From the experimental shear bending processes of TA2 Ti-alloy thin-walled tubes, it can be found that the larger the values of the moving die displacement H, the larger the values of all of I_t, I_d, and I_w [28]. Thus, moving die displacement is an important parameter for estimating tube forming limits in these processes.

Given the tube diameter D, the wall thickness t and the tube constitutive parameters, the forming indices, can be defined as follows:

$$\begin{cases} I_t = f_1(r_i, r_o, H, R_b, D_m, \mu_{tm}, \mu_{tf}, T) \\ I_d = f_2(r_i, r_o, H, R_b, D_m, \mu_{tm}, \mu_{tf}, T) \\ I_w = f_3(r_i, r_o, H, R_b, D_m, \mu_{tm}, \mu_{tf}, T) \end{cases} \quad (5)$$

The forming limits H_{max} are determined as follows:

$$H_{max} = \varphi\left(r_i, r_o, R_b, D_m, \mu_{tm}, \mu_{tf}, T, I_t^*, I_d^*, I_w^*\right) \quad (6)$$

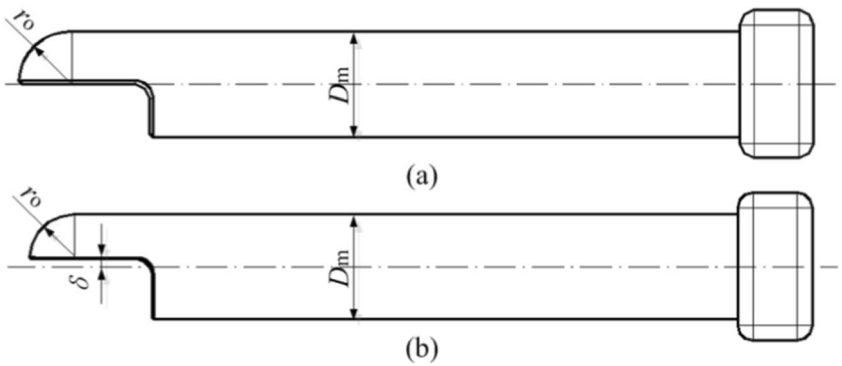

Fig. 4 Geometrical structures of mandrels

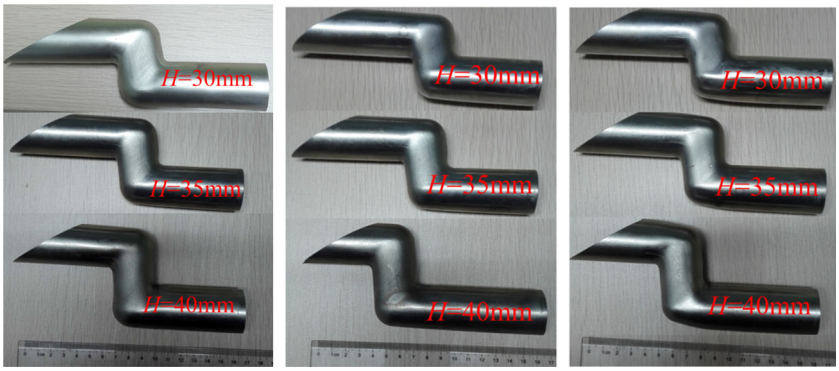

Fig. 5 Experimental tube parts

(a) r_o= 14.18 mm (b) r_o= 12.18 mm (c) r_o= 10.18 mm

where I_t*, I_d*, and I_w* are the critical values of the forming indices respectively, and the other parameters are described in Table 3.

2.3.2 Thermal-mechanical-coupled FE model

A three-dimensional (3D) elastic-plastic thermal-mechanical-coupled FE model for simulating shear bending processes of TA2 Ti-alloy thin-walled tubes under differential temperature fields is established based on the dynamic, explicit, thermal-mechanical module in ABAQUS software environment. Figure 6 shows a representative FE model for simulating these processes. In this model, half bodies of the cavities of the tube and the forming dies are modeled considering their geometrical symmetry. The tube is a deformable body discretized by the 1 mm × 1 mm thermal-mechanical eight-node doubly curved thin shell elements considering reduced integration and hourglass control. The forming dies are simplified as the rigid bodies, with constraints, discretized by the same thin shell elements.

The material model used in the simulations is an isotropic, homogeneous, elastic-plastic material following von-Mises yield criterion, with isotropic work hardening and without the Bauschinger effects taken into account.

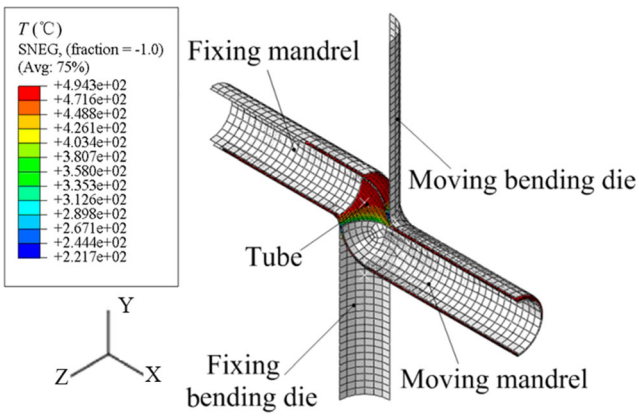

Fig. 6 A representative FE model for simulating shear bending process of Ti-alloy thin-walled tube under differential temperature fields

The displacements of the fixing bending die and the fixing mandrel are 0 mm along all freedom degree directions, while a shear velocity is exerted on the moving bending die and the moving mandrel only along the *Y* direction. The displacement of the tube's symmetrical central plane is 0 mm only along the *Z* direction, and the ones along the other directions are unconstrained.

The contact behaviors between the fixing/moving mandrels and the tube inside surface and/or between the fixing/moving bending dies and the tube outside surface are respectively simulated by using a contact pair algorithm. The tangent behaviors between them are described by the Coulomb friction model [33]. The friction heat generation is considered in the definitions of the contact properties between them.

The values of the initial temperature fields of the tube and the forming dies are the same as their preheating temperatures, and their distributions are simplified as the uniformity without considering the thermal resistances of the dies. Simulations of changes of the tube temperature fields are performed by defining the heat transfer parameters in heat conduction processes between the tube and the different dies, heat convection processes between the tube and its ambience, and thermal radiation processes between them. The relationships between the "clearance" and the "conduction coefficient" are used to define heat conduction. Both the "temperature difference" and the "convection coefficient" are used to define heat convection. Both the "temperature difference" and the "radiation coefficient" are used to define thermal radiation.

In ref. [30], the reliabilities of this FE model have been certified by the experimental results.

2.3.3 Response surface design

Experiment schemes are determined based on response surface designs, and the polynomial regression models corresponding to I_t, I_d, and I_w are developed respectively by

analyzing the experimental results. Thus, the Eq. (5) can be shown as follows:

$$I_t = \beta'_0 + \sum_{j=1}^{q} \beta'_j x_j + \sum_{h<j} \beta'_{hj} x_h x_j + \sum_{j=1}^{q} \beta'_{jj} x_j^2 \quad (7)$$

$$I_d = \beta''_0 + \sum_{j=1}^{q} \beta''_j x_j + \sum_{h<j} \beta''_{hj} x_h x_j + \sum_{j=1}^{q} \beta''_{jj} x_j^2 \quad (8)$$

$$I_w = \beta'''_0 + \sum_{j=1}^{q} \beta'''_j x_j + \sum_{h<j} \beta'''_{hj} x_h x_j + \sum_{j=1}^{q} \beta'''_{jj} x_j^2 \quad (9)$$

where (β'_0, β''_0, β'''_0) are the constants; (β'_j, β''_j, β'''_j) are the coefficients of the linear items; (β'_{hj}, β''_{hj}, β'''_{hj}) are the ones of the cross-correlation items; (β'_{jj}, β''_{jj}, β'''_{jj}) are the ones of quadratic items; x_j is the processing parameter; j is its number; and q is the parameter totality.

The experiment totality N is as follows:

$$N = 2^q + 2q + 3 \quad (10)$$

where the first item defines the experiment numbers corresponding to two levels(+1, −1)of all x_j; the second item defines the ones corresponding to two levels (+r, −r)of all x_j, where r is the distance from the 0 point; the third item defines the ones corresponding to the 0 levels of all x_j [34].

2.3.4 Predictions of forming limits

Figure 7 shows a method for predicting forming limits in Ti-alloy thin-walled tube shear bending processes under differential temperature fields. The reliable multi-index response surface models are developed firstly, by coupling the explicit thermal-mechanical FE models for simulating these bending processes with the response surface designs. Then, isolines

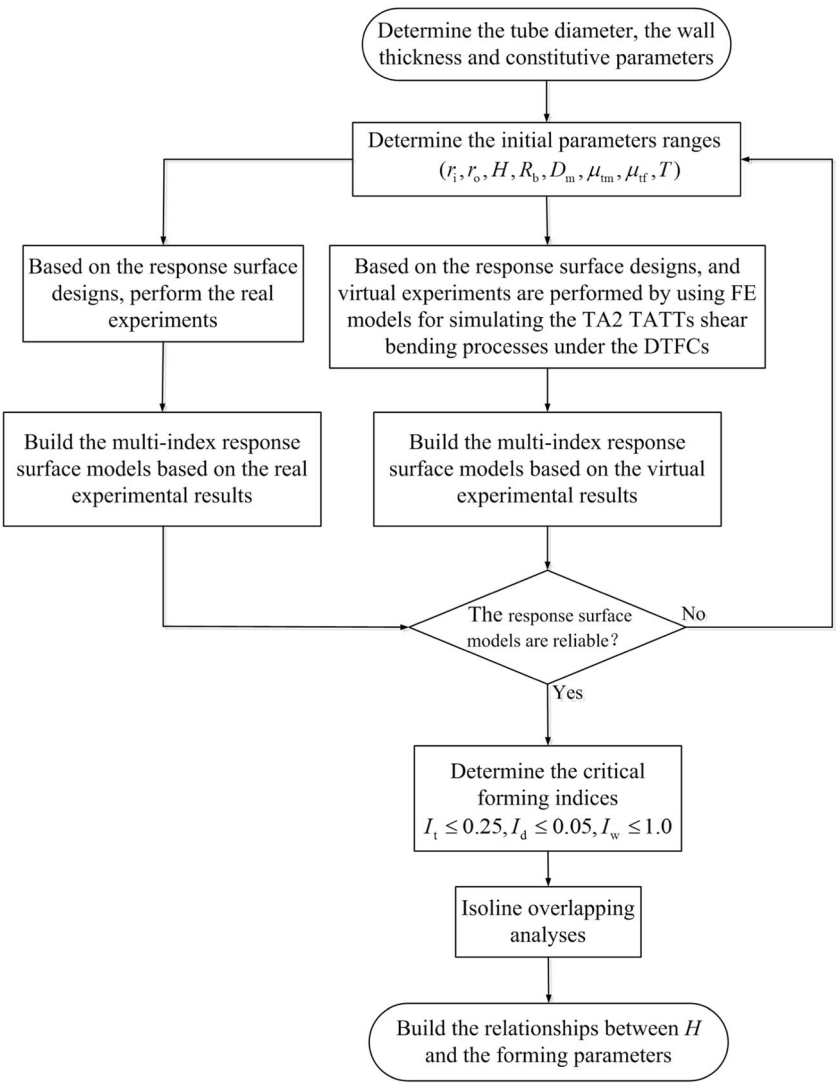

Fig. 7 Prediction method for forming limits in shear bending process of Ti-alloy thin-walled tube under differential temperature fields

overlapping analyses are performed according to the critical index values. Lastly, the relationships between the moving die displacement H and the processing parameters are developed, from which the forming limits, i.e., the maximum moving die displacement H_{max} and the feasible region ranges of the parameters are determined.

2.4 Response surface models of multi-indice

2.4.1 Response surface models

Based on the experimental parameters listed in Table 3, the response surface designs are performed under the different combinations of the inner corner radius r_i with the outer corner radius r_o. The multi-index response surface models are developed by using thermal-mechanical FE models for simulating the TA2 tube shear bending processes, and are shown as follows:

when r_i = 4 mm and $r_o = 0.5D_m$ mm,

$$\begin{cases} I_t = 40.8586 + 0.0639H - 2.0769D_m - 1.5496R_b + 0.0001H^2 + 0.0385{D_m}^2 \\ \quad + 0.0473{R_b}^2 - 0.0023HD_m \\ I_d = 2.77982 - 0.03688H - 0.00297D_m - 0.17579R_b - 0.00009H^2 + 0.00289HR_b \\ I_w = -196.71 + 1.129H + 1.495D_m + 18.737R_b - 0.569{R_b}^2 - 0.039HD_m \end{cases} \tag{11}$$

when r_i = 4 mm, and $r_o = 0.5D_m$–2 mm,

$$\begin{cases} I_t = -458.123 + 0.151H + 24.124D_m + 13.763R_b - 0.427{D_m}^2 - 0.406{R_b}^2 - 0.007HR_b \\ I_d = 18.0815 + 0.0101H - 0.6105D_m - 1.0830R_b - 0.0001H^2 + 0.0361D_mR_b \\ I_w = -189.514 + 0.658H + 1.058D_m + 19.579R_b + 0.002H^2 - 0.592{R_b}^2 - 0.027HD_m \end{cases} \tag{12}$$

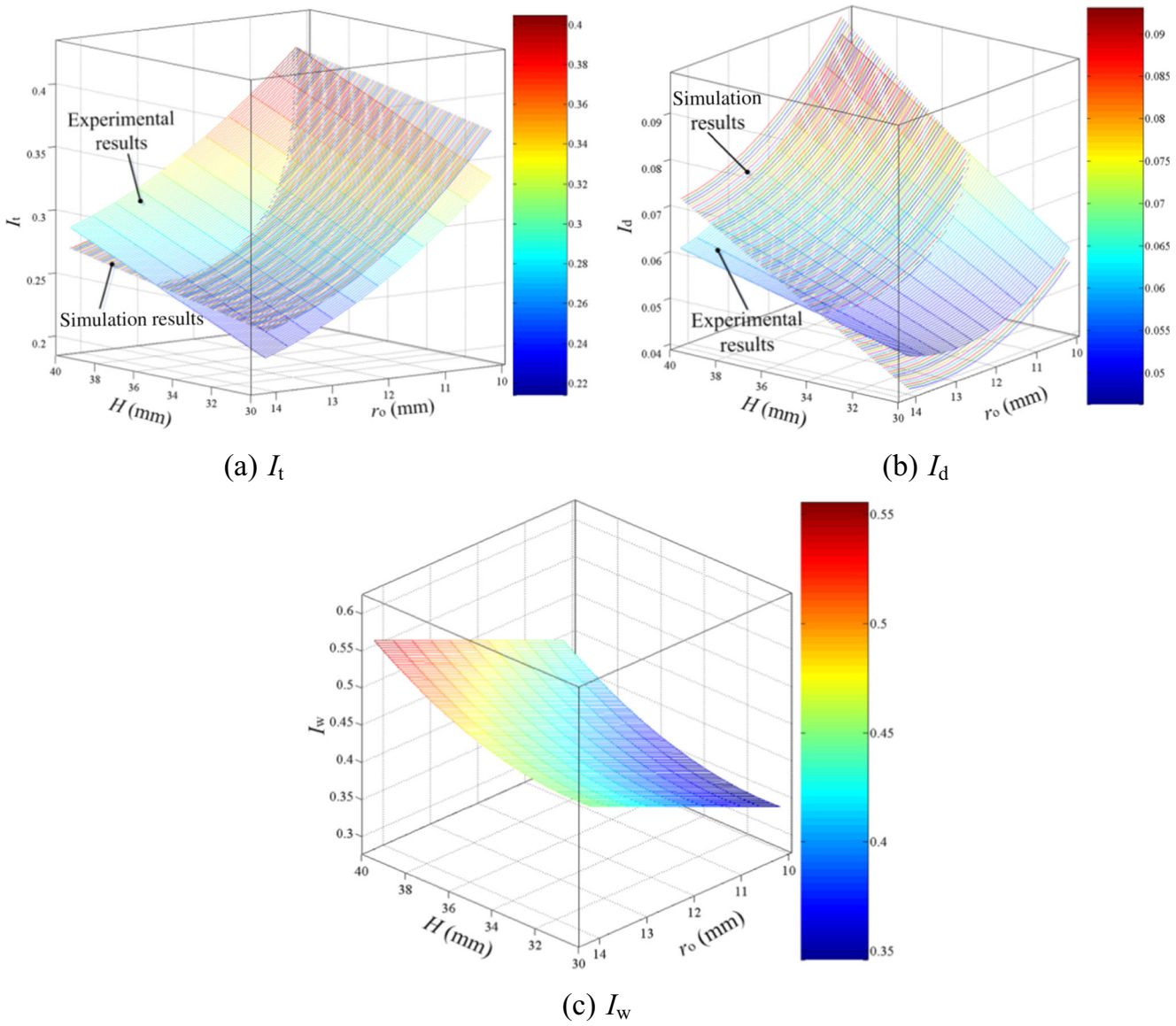

(a) I_t (b) I_d

(c) I_w

Fig. 8 Comparisons between experimental response surface models and simulation ones

When r_i = 4 mm, and $r_o = 0.5D_m$–4 mm,

$$\begin{cases} I_t = -600.120 + 0.001H + 42.454D_m - 0.064R_b - 0.749{D_m}^2 \\ I_d = -29.9620 + 0.0295H + 0.0015D_m + 3.5860R_b - 0.0003H^2 - 0.1095{R_b}^2 \\ I_w = -1269.87 - 1.14H + 63.28D_m + 47.61R_b - 1.12{D_m}^2 - 1.52{R_b}^2 + 0.08HR_b \end{cases} \quad (13)$$

When r_i = 6 mm, and $r_o = 0.5D_m$,

$$\begin{cases} I_t = 0.9396 - 0.0456H + 0.0207D_m - 0.0832R_b - 0.0029HR_b \\ I_d = 2.6698 - 0.0332H - 0.0031D_m - 0.1706R_b - 0.0001H^2 + 0.0027HR_b \\ I_w = -19.5445 + 0.5431H + 0.7375D_m - 0.1182R_b - 0.0183HD_m \end{cases} \quad (14)$$

when r_i = 8 mm, and $r_o = 0.5D_m$ mm,

$$\begin{cases} I_t = -305.428 + 0.027H + 15.589D_m + 10.138R_b - 0.275{D_m}^2 - 0.305{R_b}^2 \\ I_d = -2.50188 + 0.09182H + 0.12095D_m - 0.06053R_b - 0.00312HD_m \\ I_w = -31.3960 + 0.8945H + 1.0836D_m - 0.0798R_b - 0.0012H^2 - 0.0278HD_m \end{cases} \quad (15)$$

2.4.2 Verifications of response surface models

According to the experimental results listed in Table 4, the response surface models based on the forming indices *I*t and *I*d are developed and shown as follows:

$$\begin{cases} I_t = 0.9392 + 0.0072H - 0.1165r_o + 0.0035{r_o}^2 \\ I_d = 0.0325 + 0.0093H - 0.0237r_o + 0.0016{r_o}^2 - 0.0006Hr_o \end{cases} \quad (16)$$

From Eqs. (11)–(13), the simulation response surface models corresponding to the experimental conditions based on the forming indices *I*t, *I*d, and *I*w can be acquired and shown as follows:

$$\begin{cases} I_t = 1.4317 + 0.0035H - 0.1713r_o + 0.0056{r_o}^2 \\ I_d = 0.0778 + 0.0072H - 0.0287r_o + 0.0014{r_o}^2 - 0.0003Hr_o \\ I_w = 1.1519 - 0.0713H + 0.0283r_o + 0.0012H^2 \end{cases} \quad (17)$$

Figure 8 shows the comparisons between the experimental response surface models and simulation results. It can be found that the change tendencies of the simulation results are basically identical with the experimental ones. The maximum relative error of I_t between them is about 12% (see Fig. 8a), and the one of I_d is about 19% (see Fig. 8b). From Fig. 8c, it can be found that the $I_w < 1$ indicating the tubes are not

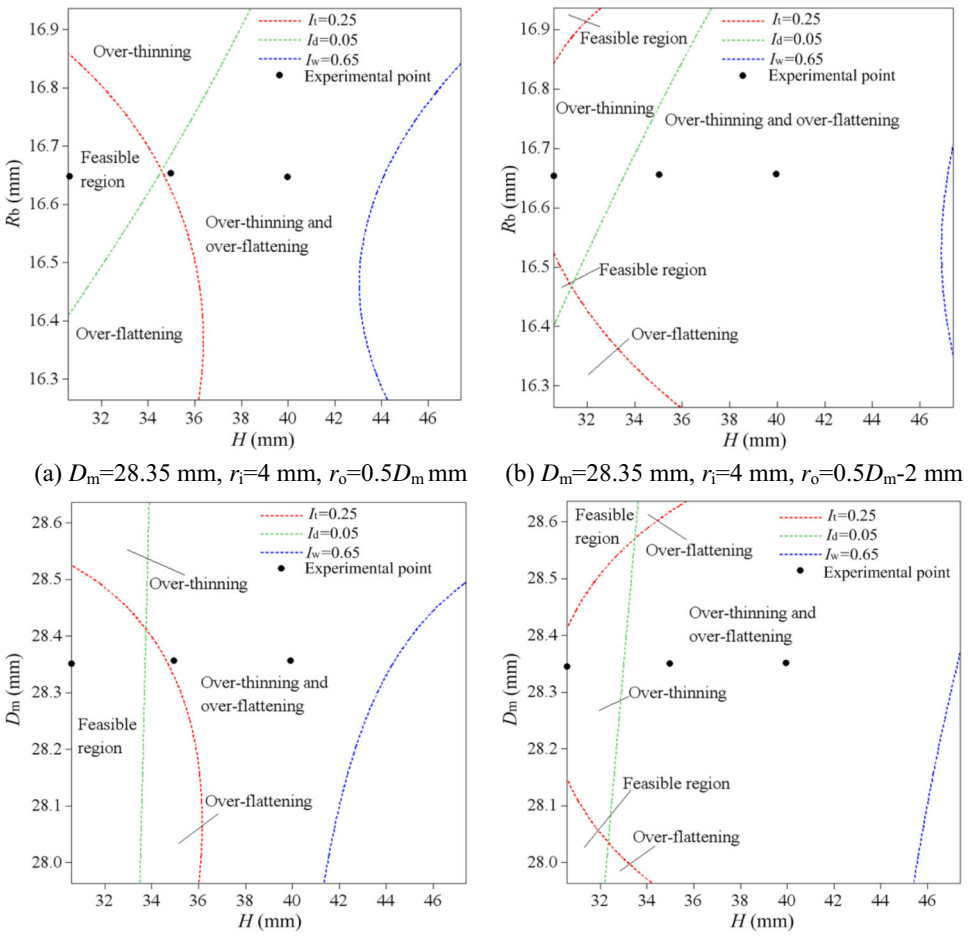

(a) D_m=28.35 mm, r_i=4 mm, r_o=0.5D_m mm

(b) D_m=28.35 mm, r_i=4 mm, r_o=0.5D_m-2 mm

(c) R_b=16.65 mm, r_i=4 mm, r_o=0.5D_m mm

(d) R_b=16.65 mm, r_i=4 mm, r_o=0.5D_m-2 mm

Fig. 9 Effects of outer corner radius on forming limits

wrinkling, which are the same as the experimental results. Thus, the reliabilities of the simulation response surface models of the multi-indice are certified.

3 Results and discussions

Based on Eqs. (11)–(15), the TA2 tube multi-index constrained forming limits are determined by using the isolines overlapping analyses.

3.1 Effects of outer corner radii

Figure 9 shows the effects of the outer corner radius r_o on the forming limit H_{max}. It can be found from Fig. 9a that when the feasible region of the bending die cavity radius $R_b \in$[16.50 mm, 16.80 mm], H_{max} = 32.00 mm; with increasing values of the moving die displacement H, feasible region ranges of R_b gradually decrease until a point. When R_b = 16.66 mm, its feasible region is a point and H_{max} = 34.50 mm reaches a peak value. When $R_b \in$[16.42 mm, 16.66 mm], the value of H_{max} depends on the over-flattening; when $R_b \in$[16.66 mm, 16.80 mm], the value of H_{max} depends on the over-thinning. Both feasible region ranges are basically consistent.

It can be found from Fig. 9b that with decreasing values of r_o, come the much smaller feasible region ranges of R_b; when H = 32.00 mm, there is no feasible region. When R_b = 16.47 mm, its feasible region is a point and H_{max} = 31.00 mm reaches a peak value. When $R_b \in$[16.40 mm, 16.47 mm], the value of H_{max} depends on the over-flattening; when $R_b \in$[16.47 mm, 16.52 mm]∪[16.85 mm, 16.90 mm], the value of H_{max} depends on the over-thinning.

It can be found from Fig. 9c that when the feasible region of the mandrel diameter $D_m \in$[28.00 mm, 28.49 mm], H_{max} = 32.00 mm; with increasing values of H, feasible region ranges of D_m gradually decrease until a point. When D_m = 28.46 mm, its feasible region is a point and H_{max} = 33.75 mm reaches the peak value. When $D_m \in$[28.00 mm, 28.41 mm], the value of H_{max} depends on the over-flattening; when $D_m \in$[28.41 mm, 28.53 mm], the value of H_{max} depends on the over-thinning.

It can be found from Fig. 9d that with decreasing values of r_o, come smaller feasible region ranges of D_m; when $D_m \in$[28.00 mm, 28.05 mm]∪[28.51 mm, 28.60 mm], H_{max} = 32.00 mm. When D_m = 28.57 mm, its feasible region

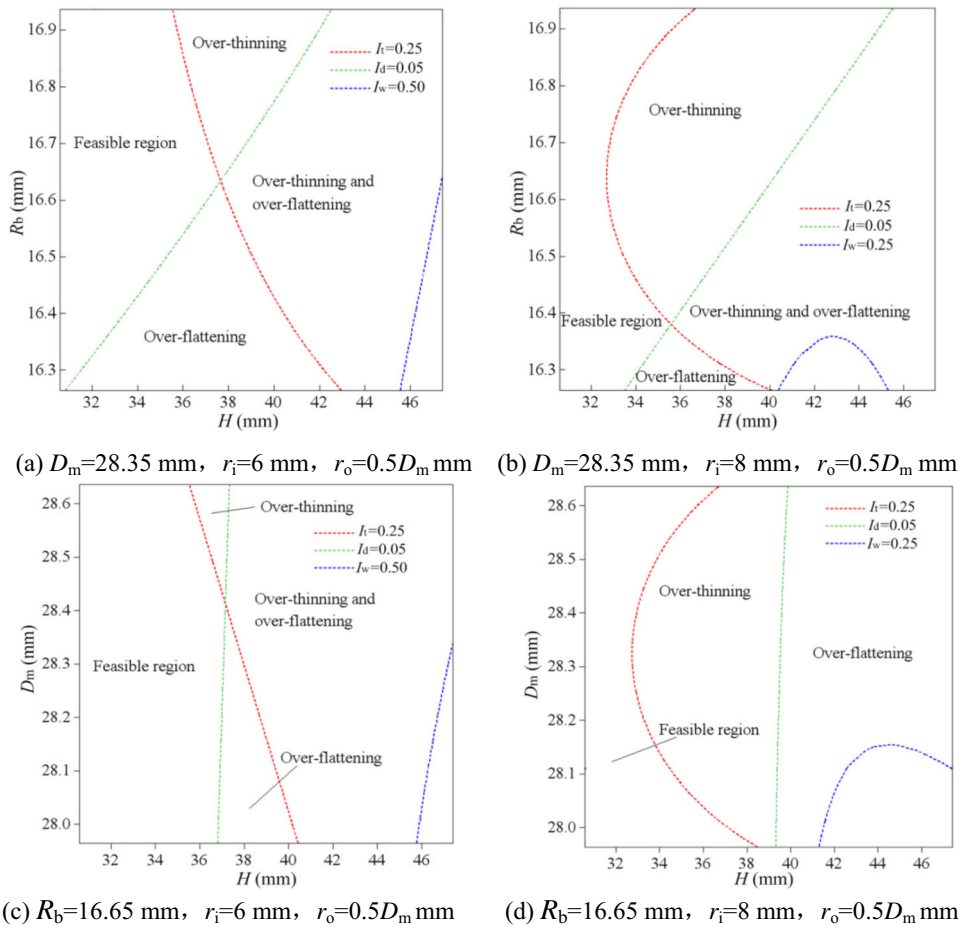

(a) D_m=28.35 mm, r_i=6 mm, r_o=0.5D_m mm (b) D_m=28.35 mm, r_i=8 mm, r_o=0.5D_m mm

(c) R_b=16.65 mm, r_i=6 mm, r_o=0.5D_m mm (d) R_b=16.65 mm, r_i=8 mm, r_o=0.5D_m mm

Fig. 10 Effects of inner corner radius on forming limits

is a point and H_{max} = 33.46 mm reaches a peak value. When D_m∈[28.00 mm, 28.14 mm]∪[28.42 mm, 28.57 mm], the value of H_{max} mainly depends on the over-thinning. Thus, the effects of the bending die cavity radius on the forming limits are larger than the mandrel diameter.

The tube forming qualities under the experimental conditions can be determined from Fig. 9, and the predicted defects are the same as the experimental results (see Table 4).

3.2 Effects of inner corner radii

Figure 10 shows the effects of the inner corner radius r_i on the forming limit H_{max}. It can be found from Fig. 10a that with increasing values of r_i, come larger feasible region ranges of R_b; when the feasible region of R_b∈[16.33 mm, 16.90 mm], H_{max} = 32.00 mm. When R_b = 16.63 mm, its feasible region is a point and H_{max} = 37.65 mm reaches a peak value. When R_b∈[16.30 mm, 16.63 mm], the value of H_{max} depends on the over-flattening; when R_b∈[16.63 mm, 16.90 mm], the value of H_{max} depends on the over-thinning.

It can be from Fig. 10b that with increasing values of r_i, come larger feasible region ranges of R_b, but their increments defined as the changes of the values of parameter feasible region area are small; when the feasible region of R_b∈[16.26 mm, 16.90 mm], H_{max} = 32.00 mm. When R_b = 16.38 mm, its feasible region is a point and H_{max} = 35.56 mm reaches a peak value. When R_b∈[16.30 mm, 16.38 mm], the value of H_{max} depends on the over-flattening; when R_b∈[16.38 mm, 16.90 mm], the value of H_{max} depends on the over-thinning and its ranges are larger than the former.

It can be from Fig. 10c that when the feasible region of D_m∈[28.00 mm, 28.60 mm], H_{max} = 34.00 mm; when D_m = 28.41 mm, its feasible region is a point and H_{max} = 37.16 mm reaches a peak value. When D_m∈[28.00 mm, 28.41 mm], the value of H_{max} depends on the over-flattening; when D_m∈[28.41 mm, 28.60 mm], the value of H_{max} depends on the over-thinning.

It can be from Fig. 10d that with increasing values of r_i, come smaller feasible region ranges of D_m; when the feasible region of D_m∈[28.00 mm, 28.14 mm]∪[28.51 mm, 28.60 mm], H_{max} = 34.00 mm. When D_m = 28.00 mm, its feasible region is a point and H_{max} = 37.16 mm reaches a peak value.

4 Conclusions

1. A method for predicting the multi-index constrained forming limits in shear bending processes of Ti-alloy thin-walled tubes under differential temperature fields was presented by coupling an explicit thermal-mechanical-coupled FE model for simulating these processes and utilizing the response surface design method. The reliable multi-index response surface models corresponding to the maximum thinning ratio, the maximum ovality, and the wrinkling factor were developed for the TA2 Ti-alloy thin-walled tubes, and their forming limits, i.e., the maximum moving die displacements, were predicted.
2. The peak values of the maximum moving die displacement are located in the convexes of the processing parameter's feasible regions. The smaller the values of the outer corner radius, the smaller both the values of forming limits and the feasible region ranges of the bending die cavity radius and the mandrel diameter; the feasible region changes of the bending die cavity radius are larger than the mandrel diameter. With the increases of the inner corner radius, their feasible region ranges increase firstly and then keep stable; the values of the maximum moving die displacement increase. When the value of the outer corner radius is a half of the mandrel diameter and the value of the inner corner radius is from 4 to 6 mm, their feasible region ranges are the maximum.
3. The values of the maximum moving die displacement for the present conditions depend on the over-thinning or the over-flattening. For the value of the inner corner radius is 4 mm, when the feasible region of the bending die cavity radius is from 16.42 to 16.66 mm, the value of the forming limit depends on the over-flattening; when its feasible region is from 16.66 to 16.80 mm, the value of the forming limit depends on the over-thinning. For the value of the inner corner radius is 6 mm, when its feasible region is from 16.30 to 16.63 mm, the value of the forming limit depends on the over-flattening; when its feasible region is from 16.63 to 16.90 mm, the value of the forming limit depends on the over-thinning. For the value of the inner corner radius is 8 mm, when its feasible region is from 16.30 to 16.38 mm, the value of the forming limit depends on the over-flattening; when its feasible region is from 16.38 to 16.90 mm, the value of the forming limit depends on the over-thinning.
4. For the value of the inner corner radius is 4 mm, when the feasible region of the mandrel diameter is from 28.00 to 28.41 mm, the value of the forming limit depends on the over-flattening; when its feasible region is from 28.41 to 28.53 mm, the value of the forming limit depends on the over-thinning. For the value of the inner corner radius is 6 mm, when its feasible region is from 28.00 to 28.41 mm, the value of the forming limit depends on the over-flattening; when its feasible region is from 28.41 to 28.60 mm, the value of the forming limit depends on the over-thinning. For the value of the inner corner radius is 8 mm, when its feasible region is from 28.00 to 28.60 mm, the value of the forming limit only depends on the over-thinning.

The method for predicting multi-index constrained forming limits presented in this study provides a scientific base for understanding and predicting forming limits in shear bending

processes of Ti-alloy thin-walled tubes under differential temperature fields. Meanwhile, the results enable improvements of the forming limits of the TA2 tubes.

Acknowledgements The authors would like to gratefully acknowledge the support of National Natural Science Foundation of China (No. 51305415).

References

1. Yang H, Li H, Zhang ZY, Zhan M, Liu J, Li GJ (2012) Advances and trends on tube bending forming technologies. Chin J Aeronaut 25:1–12. doi:10.1016/S1000-9361(11)60356-7
2. Li H, Yang H, Liu K (2013) Towards an integrated robust and loop tooling design for tube bending. Int J Adv Manuf Technol 9–12: 1303–1318. doi:10.1007/s00170-012-4258-1
3. Lazarescu L (2013) Effect of internal fluid pressure on quality of aluminum alloy tube in rotary draw bending. Int J Adv Manuf Technol 64:85–91. doi:10.1007/s00170-012-3992-8
4. Zhang ZY, Yang H, Li H, Tao ZJ (2014) Thermo-mechanical coupled 3D-FEmodeling of heat rotary draw bending for large diameter thin-walled CP-Ti tube. Int J Adv Manuf Technol 72:1187–1203. doi:10.1007/s00170-014-5709-7
5. Yan J, Yang H, Zhan M, Li H (2010) Forming characteristics of Al-alloy large diameter thin-walled tubes in NC-bending under axial compressive loads. Chin J Aeronaut 23:461–469. doi:10.1016/S1000-9361(09)60242-9
6. Zeng YS, Li ZQ (2002) Experimental research on the tube push-bending process. J Mater Proc Technol 122:237–240. doi:10.1016/S0924-0136(02)00027-4
7. Li SH, He J, Cedric Z, Zeng D, Hou B (2014) Bifurcation analysis of forming limits for an orthotropic sheet metal. J Manuf Sci Eng, Trans ASME 135:1–10. doi:10.1115/1.4027757
8. Li HZ, Wu X, Li GY (2013) Prediction of forming limit diagrams for 22MnB5 in hot stamping process. J Mater Eng Perform 22: 2131–2140. doi:10.1007/s11665-013-0491-5
9. Hashemi R, Madoliat R, Afshar A (2014) Prediction of forming limit diagrams using the modified M-K method in hydroforming of aluminum tubes. Int J Mater Form. doi:10.1007/s12289-014-1207-6
10. Eyckens P, Bael AV, Houtte PV (2009) Marciniak–Kuczynski type modelling of the effect of through-thickness shear on the forming limits of sheet metal. Int J Plast 25:2249–2268. doi:10.1016/j.ijplas.2009.02.002
11. Butuca MC, Gracioa JJ, Barata RA (2006) An experimental and theoretical analysis on the application of stress-based forming limit criterion. Int J Mech Sci 48:414–429. doi:10.1016/j.ijmecsci.2005.11.007
12. Sun ZC, Yang H (2007) Study on forming limit and feasibility of tube axial compressive process. J Mater Proc Technol 187–188: 292–295. doi:10.1016/j.jmatprotec.2006.11.102
13. Yang H, Lin Y (2004) Wrinkling analysis for forming limit of tube bending processes. J Mater Process Technol 152:363–369. doi:10.1016/j.jmatprotec.2004.04.410
14. Liu G, Peng JY, Yuan SJ, Teng BG, Li K (2015) Analysis on critical conditions of sidewall wrinkling for hydroforming of thin-walled Tee-joint. Int J Machin Tools Manuf 97:42–49. doi:10.1016/j.ijmachtools.2015.06.004
15. Bagheriasl R, Worswick MJ (2015) Formability of AA3003 brazing sheet at elevated temperatures: limiting dome height experiments and determination of forming limit diagrams. Int J Mater Form 8: 229–244. doi:10.1007/s12289-014-1162-2
16. Yang LF, Hu GL, Liu JW (2015) Investigation of forming limit diagram for tube hydroforming considering effect of changing strain path. Int J Adv Manuf Technol 79:793–803. doi:10.1007/s00170-015-6842-7
17. Sun T, Liang J, Guo X, Ren MD, Wang LZ (2015) Optical measurement of forming limit and formability of Cu/Al clad metals. J Mater Eng Perform 24:1426–1433. doi:10.1007/s11665-015-1435-z
18. Narayanasamy R, Loganathan C (2006) Study on wrinkling limit of commercially pure aluminium sheet metals of different grades when drawn through conical and tractrix dies. Mater Sci Eng A 419:249–261. doi:10.1016/j.msea.2005.12.026
19. Li FF, Fu MW, Lin JP, Wang XN (2014) Experimental and theoretical study on the hot forming limit of 22MnB5 steel. Int J Adv Manuf Technol 71:297–306. doi:10.1007/s00170-013-5468-x
20. Chu XR, Leotoing L, Guines D, Ragneau E (2015) Effect of material thermo-viscoplastic modeling on the prediction of forming limit curves of aluminum alloy 5086. J Mater Eng Perform 24:3459–3470. doi:10.1007/s11665-015-1643-6
21. Xiao YH, Liu YL, Yang H (2014) Prediction of forming limit based on cross-sectional distortion for rotary draw bending of H96 brass double-ridged rectangular tube. Int J Adv Manuf Technol 71:1445–1454. doi:10.1007/s00170-013-5552-2
22. Nguyen DT, Kim YS (2013) A numerical study on establishing the forming limit curve and indicating the formability of complex shape in incremental sheet forming process. Int J Precis Eng Manuf 14: 2087–2093. doi:10.1007/s12541-013-0283-8
23. Lee JW, Kwon HC, Rhee MH, Im YT (2003) Determination of forming limit of a structural aluminum tube in rubber pad bending. J Mater Process Technol 140:487–493. doi:10.1016/S0924-0136(03)00775-1
24. Yan J, Yang H, Zhan M, Li H (2010) Forming limits under multi-index constraints in NC bending of aluminum alloy thin-walled tubes with large diameters. Sci China Tech Sci 53:326–342. doi:10.1007/s11431-009-0331-x
25. Sivasankaran S, Narayanasamy R, Jeyapaul R, Loganathan C (2009) Modelling of wrinkling in deep drawing of different grades of annealed commercially pure aluminium sheets when drawn through a conical die using artificial neural network. Mater Des 30:3193–3205. doi:10.1016/j.matdes.2009.01.020
26. Zemin F, Jianhua M, Chen L, Chen W (2010) Using genetic algorithm-back propagation neural network prediction and finite-element model simulation to optimize the process of multiple-step incremental air-bending forming of sheet metal. Mater Des 30:267–277. doi:10.1016/j.matdes.2009.06.019
27. Wei DL, Zhen ZS, Chen J (2009) Optimization and tolerance prediction of sheet metal forming process using response surface model. Comput Mater Sci 42:228–233. doi:10.1016/j.commatsci.2007.07.014
28. Yan J (2016) Plastic wrinkling model and characteristics of shear enforced titanium alloy thin-walled tubes under combination die constraints and differential temperature fields. Chin J Aeronaut doi:10.1016/j.cja. 2016.06.019
29. Editor commitee of "China aeronautical materials handbook" (2001) *China aeronautical materials handbook*. China standard press Beijing, pp 10–20 (in Chinese)
30. Yan J, Wu W (2016) Identification method of shear stress constitutive parameters of Ti-alloy thin-walled tube. Acta Aeronautica Et Astronautica Sinica 37:2884–2894. doi:10.7527/S1000-6893.2015.0289
31. Zhao ZN (2002) Heat transfer. Higher education press, Beijing (in Chinese)
32. Li YQ, Lin ZR, Chen CK, Zhang ZY, Ying JL (1986) Ti-alloy sheet metal forming technology. Defense Industry Press, Beijing (in Chinese)
33. Hibbit K, Sorensen (2009) ABAQUS. Version 6.9. Hibbit Karlson and Sorensen Inc Washington
34. Ren LQ (2009) Regression design and its optimization. Science Press, Beijing (in Chinese)